Fuel cell electrocatalsis : oxygen reduction on Pt-based nanoparticle catalysts

Vliet, D.F. van der

Chapter 4

Monodisperse Pt_3Co Nanoparticles as Electrocatalysts: the effects of Particle Size and Pretreatment on Electrocatalytic Reduction of Oxygen

Monodisperse Pt_3Co nanoparticles have been synthesized with size control via an organic solvothermal approach. The obtained nanoparticles were incorporated into a carbon matrix and applied as electrocatalysts for the oxygen reduction reaction to investigate the effects of particle size and pretreatment on their catalytic performance. It has been found that the optimal conditions for maximum mass activity were with particles of 4.5 nm and a mild annealing temperature of about 500 ^{o}C. While the particle size effect can be correlated to the average surface coordination number, Monte Carlo simulations have been used to depict the nanoparticle structure and segregation profile, which revealed that the annealing temperature has a direct influence on the particle surface relaxation, segregation and adsorption/catalytic properties. The fundamental understanding of activity enhancement in Pt-bimetallic alloy catalysts could be utilized to guide the development of advanced nanomaterials for catalytic applications.

The contents of this chapter have been based on the article: C. Wang, G.Wang, D. van der Vliet, K.C. Chang, N.M. Markovic and V.R. Stamenkovic, *Phys. Chem. Chem. Phys.*, 12 **(2010)**, 6877

4.1 Introduction

Alloy nanoparticles (NPs) have attracted increasing interest due to their superior performance in magnetic [1-5], optical [6-8] and catalytic [9-13] applications. Particularly, Pt bimetallic alloys with transition metals (PtM with M = Fe, Co, Ni, etc.) have been found to be highly active for oxygen reduction, the troubled cathode reaction in fuel cells. [12-15] The enhancement factors for specific activity were found to be up to 3 times those on extended polycrystalline surfaces. [12] This has initiated a lot of efforts to synthesise Pt-based alloy nanoscale catalysts, which are usually in the form of PtM NPs dispersed in a high surface area carbon matrix (PtM/C). The approaches mostly include co-precipitation of metal salts in aqueous solution [16], impregnation of transition metals into Pt/carbon catalyst [17], and electrodeposition. [18, 19] Previous electrocatalytic studies for the nanocatalysts prepared via these conventional approaches under proton-exchange membrane fuel cell (PEMFC) conditions, however, failed to achieve the same level of catalytic activity as in the case of extended surfaces, *i.e.*, the specific activity at 0.9V of the nanoscale catalyst is about one order of magnitude lower than that of the extended surface of the corresponding material.[12, 14, 20-23] Nevertheless, Mukerjee *et al.* reported specific activity enhancement factors of 2–3 when using Pt–Co/C, Pt–Ni/C or Pt–Cr/C versus Pt/ C. [20, 21] Gasteiger *et al.* observed a 3-fold enhancement in specific activity for multiply-leached PtCo/C versus Pt/C in their benchmark study of oxygen reduction reaction (ORR) electrocatalysts. [14] Rotating disk electrode (RDE) studies of carbon supported alloy catalysts of similar sizes by Paulus *et al.* also showed an specific activity improvement of *ca.* 1.5 for $Pt_{0.75}Co_{0.25}$/C and $Pt_{0.75}Ni_{0.25}$/C, and a more significant enhancement of *ca.* 42 for $Pt_{0.5}Co_{0.5}$/C in comparison with Pt/C. [22, 23] These studies revealed that the alloy nanocatalysts prepared by the conventional approaches are falling behind the activities obtained on extended surfaces, and there is still much to be done to improve the quality of alloy NPs.

Meanwhile, the particle size effect is also known to play a key role in catalysis, affecting not only the activity but also the reaction mechanism, selectivity and catalyst stability. [24-26] In spite of the efforts in preparing various types of alloy catalyst, however, size-dependent activity has rarely been investigated for Pt alloy catalysts [26] compared to the extensive study in conventional Pt/C catalysts. The

challenge may lie in the size-controlled synthesis of bimetallic catalysts with monodisperse NPs of uniform composition and shape.

A promising approach toward high-quality nanomaterials for catalytic applications is the organic solution synthesis. This method has already been widely applied for synthesis of various types of nanocrystals. Not only can size be tuned from 1 nm to several hundred nanometres, but also morphology can be well controlled. [27-29] Nanomaterials from organic solution synthesis have been reported to exhibit superior functional performance in various applications. [1, 3, 30, 31] Particularly, it may be advantageous in preparation of monodisperse alloy NPs with homogeneous element distributions for catalysis. [4, 29]

The synthesis of monodisperse Pt_3Co NPs by an organic solvothermal approach is described in chapter 3. The temperature at which the Co precursor (Cobalt carbonyl, $Co_2(CO)_8$)was added, was adjusted to control the particle size from 3 to 9 nm. This has enabled the study of the particle size effect by applying these NPs as catalysts in electrocatalysis, *e.g.* the oxygen reduction reaction (ORR). Our results show that the ORR specific activity of Pt_3Co increases with the particle size, and the maximum in mass activity can be achieved with NPs of about 4.5 nm by balancing the specific surface area and specific activity. Regardless of the observed high activity and size related trends established in the previous work, other conditions of the catalyst synthesis including pretreatments have not been investigated and optimized yet. Also a deep insight into the mechanism underlying the size-dependent activity is desired for guiding further study and design of advanced catalysts. In this study, we first examine the size-dependent activity of Pt_3Co NPs for ORR and postulate the particle size effect through the change of the average coordination number of surface atoms with the particle size. We then specifically focus on the 4.5 nm Pt_3Co NPs, which have shown the highest mass activity, to study the effect of pretreatment conditions. The NPs deposited on carbon black are annealed at different temperatures and electrochemical studies are applied to clarify the effect of annealing temperature on their catalytic performance. Finally, theoretical modeling based on Monte Carlo simulation is performed for better understanding of the experimental observations.

4.2 Experimental

4.2.1 NP synthesis

The Pt_3Co NPs were synthesized through an organic solvothermal approach modified from previous publications. [32] In a typical synthesis of 4.5 nm Pt_3Co NPs, 0.16 mmol $Pt(acac)_2$ was dissolved in 10 ml oleylamine and 5 ml benzyl ether, in the presence of 1 mmol 1-tetradecanediol, 2.8 mmol 1-adamantanecarboxylic acid (ACA). The formed solution was heated to 200 ^{o}C under Ar flow and 0.25 mmol $Co_2(CO)_8$ dissolved in 1 ml dichlorobenzene was injected into this hot solution in Ar atmosphere. After 30 min, the solution temperature was raised to 260 ^{o}C and kept there for 30 min. The solution was then cooled down to room temperature and 40 ml iso-propanol and 20 ml ethanol were added to precipitate NPs, followed by centrifuging. The collected product was dispersed in 10 ml hexane for further applications. Introducing $Co_2(CO)_8$ at 225, 170 and 145 ^{o}C gave Pt_3Co NPs of 3, 6 and 9 nm, respectively.

4.2.2 Characterizations

TEM images and EDX spectra were collected on a Philips CM 30 TEM equipped with EDX functionality. The EDX analysis covered a large area of nanoparticle assembly(1 mm; over thousands of particles).

4.2.3 Electrochemical measurements

The Pt_3Co NPs of various sizes were supported on carbon black (Tanaka TKK, Tokyo: ~900 $m^2 g^{-1}$) *via* a colloidal deposition method. [26] Organic surfactants were removed by heat treatment of the NP/carbon mixture in oxygen-rich atmosphere at 185 ^{o}C. [33] The obtained catalyst was then dispersed in deionized water by vigorous sonication, and the formed suspension was pipetted on the surface of a glassy carbon (GC) electrode (6 mm in diameter). The ratio of Pt in the catalyst was tuned to 28 wt-%, and the loading of Pt on GC electrode was set at 9 μg cm^2_{disk}, with the exception of 12 μg cm^2_{disk} for 9 nm particles in order to reach proper diffusion limiting current based on the geometry of the disk. After drying under argon flow, the GC electrode was immersed into electrolyte. The

electrochemical measurements were conducted in a three-compartment electrochemical cell in a rotating disc electrode (RDE) setup. A saturated Ag/AgCl electrode and a Pt wire were used as reference and counter electrodes, respectively in 0.1 M $HClO_4$ electrolyte. Cyclic voltammogram (CV) was collected under Ar saturation with scanning rates of 20 and 50 mV s^{-1} at 20 °C, and ORR activity was measured by RDE method with scan rate of 20 mV s^{-1} at 60 °C. All potentials in this report are given versus reversible hydrogen electrode (RHE, calibrated by the H_2 oxidation reaction after each measurement), and readout currents are corrected for the ohmic iR drop. [34] The specific activity was represented as the kinetic current density (j_k) at 0.9 V vs. RHE.

4.2.4 Simulation

Monte Carlo (MC) simulation was employed in this work to derive the equilibrium surface composition of the Pt_3Co alloy NPs. In our simulation, we applied canonical ensemble statistical mechanics. Starting from an initial configuration of Pt_3Co particle with randomly distributed Pt and Co atoms, a series of configuration transformations are performed to reach the thermodynamically equilibrated states of the simulated system. At each MC step, two randomly selected atoms with different element types exchange their positions and the energy change ΔE associated with this change was then calculated using a modified embedded atom method. [35, 36] If the energy decreases ($\Delta E < 0$), we always proceed with the new configuration; while the energy increases ($\Delta E > 0$), the new configuration is retained with a probability P given by $P = \exp(\Delta E/k_B T)$. Here, k_B is the Boltzmann constant and T is the temperature. Similar approach has been successfully applied before to predict the surface segregation in Pt–Ni, [37] Pt–Re, [38] and Pt–Mo [39] NPs.

4.3 Results and discussion

The synthesized monodisperse Pt_3Co NPs with sizes controlled from 3 to 9 nm were incorporated into carbon black and applied as electrocatalysts for the ORR to study the size effect on their catalytic performance. Pretreatment conditions were also investigated by annealing the catalyst at different temperatures before the electrochemical measurements of the ORR activity. A theoretical explanation of the

observed phenomena was established based on Monte Carlo simulation of the element distribution in the NPs exposed to different treatment procedures.

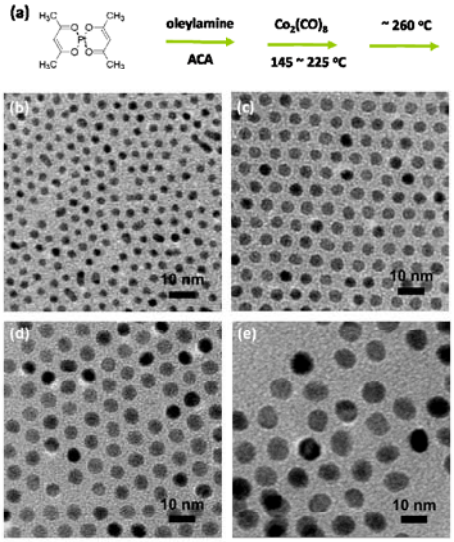

Figure 4.1 (a) Schematic illustration of the synthesis of Pt_3Co NPs via an organic solvothermal approach. (b)–(e) TEM images of 3, 4.5, 6and 9 nm Pt_3Co NPs respectively. The contrast difference among the NPs is not caused by compositional variance, but instead by the different crystalline alignment against the electron beam in imaging.

4.3.1 Size controlled synthesis of Pt_3Co NPs

Figure 4.1a illustrates the scheme of the synthesis. The platinum precursor, $Pt(acac)_2$, was dissolved in an high-boiling-point organic solvent (benzyl ether, phenyl ether, octyl ether, etc.) with the assistance of surfactants, oleylamine and ACA. Diol was added as reducing agent. The obtained mixture was heated up in an inert atmosphere (N_2 or Ar) to an elevated temperature (145–225 ^{o}C), where reduction of Pt salt started and generated Pt^{0} species. The injection of $Co_2(CO)_8$ induced an immediate change of the solution color from transparent light yellow to black, due to the fast decomposition of $Co_2(CO)_8$ and nucleation of Co with Pt. The formed nuclei were further grown into NPs by raising the temperature to 260 ^{o}C (due to the large volume ratio of oleylamine, the solution cannot be heated to reflux within the Ar saturated flask). Figure 1b–e show the representative TEM imagesof 3,4.5,6 and 9 nm Pt_3Co NPs obtained by adding Co precursor at 225, 200, 170 and 145 ^{o}C. The size of the obtained NPs could be controlled by the amount of

precursor left after the instantaneous nucleation after $Co_2(CO)_8$ was injected. For introduction of Co at a low temperature (*e.g.*, 145 °C), the nucleation rate was rather slow and thus the number of nuclei formed was small. Plenty of precursors were left for further growth, allowing the NPs to grow into big size (9 nm). In contrast, at a high injection temperature (*e.g.*, 200 °C), most of the precursor was consumed by the boosted nucleation and a large number of nuclei formed, and therefore, only NPs of small size (3 nm) can be obtained. [10] A similar mechanism has also been applied to explain the size control of other NPs growing in organic solution. [40, 41]

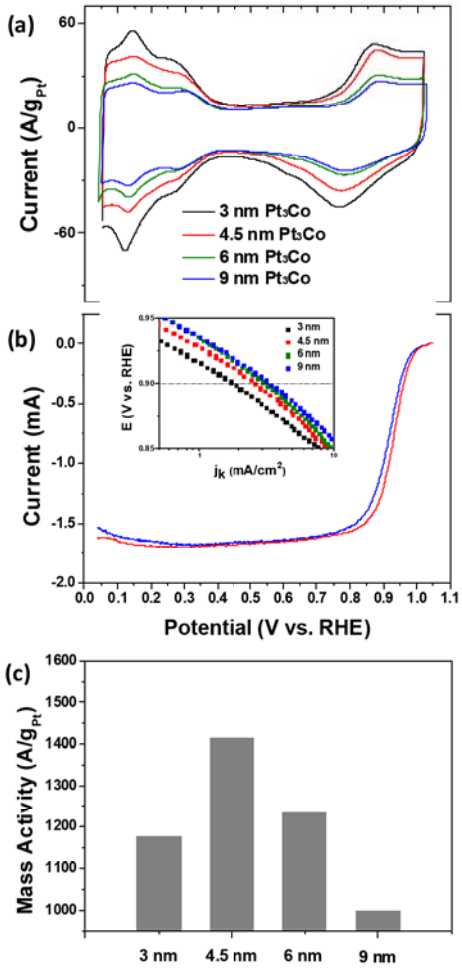

Figure 4.2 (a) Voltammograms and (b) polarization curves recorded for Pt_3Co NP catalysts of various sizes, with the inset showing the corresponding Tafel plots. (c) The summary of mass activity vs. particle size.

4.3.2 Size-dependent activity

The particle size effect for a Pt catalyst has been well known from the literature. [24, 25] Though disputations still exist, [42] it is generally accepted that the mechanism of Pt-size effect is due to enhanced adsorption of oxygenated species (OH_{ad} formed from oxidation of water) on smaller particles with decreased average coordination numbers [25], and consequently more pronounced oxophilic behavior. It is shown here that the particle size effect also exists in Pt bimetallic alloy catalysts. From the voltammograms depicted in figure 4.2a, it is found that the H_{upd} region (0.05 V < E < 0.4 V vs. RHE) shrinks as the size of the NPs increases from 3 to 9 nm, indicating a reduced specific surface area owing to the increase of particle size. The specific activities measured by RDE increase in the following trend: 3 < 4.5 < 6 < 9 nm (figure 4.2b), with the activity of 9 nm being twice that for 3 nm Pt_3Co NPs. It should be noted that, during operation in a low pH environment such as PEMFC, all of the surface Co atoms would be dissolved immediately resulting in skeleton type of surface morphology with low coordinated Pt topmost atoms. [12] The level of catalytic enhancement is thus likely to depend on the Co concentration in the subsurface layers and the extent of surface Pt coordination. By balancing these two opposite trends, i.e. smaller surface area and higher specific activity as particle size increases, the maximum mass activity has been achieved with 4.5 nm Pt_3Co NPs (figure 4.2c). The catalyst with this size was hence in the focus of the following studies.

4.3.3 Annealing temperature

Pretreatment of the catalyst by annealing is an important procedure in alloy catalyst preparation. This is usually carried out in vacuum or a reducing atmosphere (H_2, CO, etc.) and the general purpose is to homogenize the alloy composition. However, annealing always comes together with sintering of NPs. Lack of control over size, alloy homogeneity and crystal structure of catalyst particles has made it ambiguous in previous studies for annealing effect. [21, 43, 44] The monodisperse and homogeneous Pt_3Co NPs prepared here, however, have enabled a systematic study of the annealing effect on catalytic performance for bimetallic alloy nanoscale catalyst. Based on the established activity dependence versus particle size, we were

able to distinguish the effect of annealing from size and thus to rule out the intrinsic contribution of the pretreatment on activity enhancement.

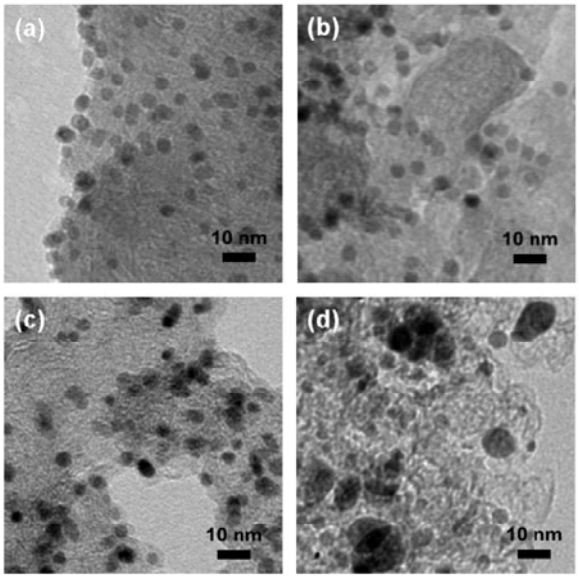

Figure 4.3, TEM images of (a) as prepared, and (b) 400 °C, (c) 500 °C, (d) 800 °C annealed 4.5 nm Pt_3Co/C catalysts.

The as-prepared (figure 4.3a) 4.5 nm Pt_3Co/C catalyst was treated for annealing procedures at various temperatures ranging from 300 to 800 °C (in Ar + 5% H_2). No obvious size or morphology change was observed for the catalysts annealed up to 400 °C (figure 4.3b). Particle sintering appeared for the catalyst annealed at temperatures higher than 500 °C, yet was not significant at this temperature (figure 4.3c) but evident at 800 °C (figure 4.3d). In the latter case, agglomeration of particles with sizes over 20 nm has been observed. The observed trend of size change was verified by XRD analysis. Figure 4.4a shows the XRD patterns recorded for as prepared and various annealed catalysts. All the patterns show characteristic peaks of Pt_3Co crystal in disordered fcc phase. [26, 44] According to the Scherrer equation, crystalline size in the catalyst can be calculated from the peak width in the XRD pattern. The results corresponding to the calculation for (111) peak were depicted in figure 4.4b. Consistent with the observation from TEM, the size enlargement was insignificant for annealing up to 500 °C, while the average particle size increased to ~6 nm for 600 °C and ~13 nm for 800 °C annealing. Unlike the report by Schulenburg *et al.* [44], our catalysts show single crystal phase

under annealing, conforming the homogeneous alloy composition in the fcc Pt_3Co NPs. The exclusion of crystal phase alteration in addition thus allows exploration of the intrinsic effect of annealing on the catalytic performance of the catalyst.

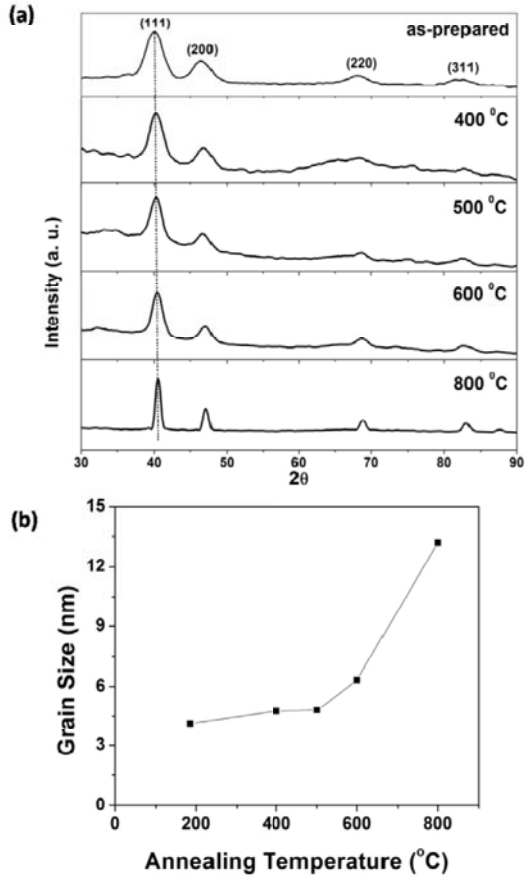

Figure 4.4 (a) XRD patterns of the 4.5 nm Pt_3Co/C catalysts at various treatment stages. (b) Crystal grain size corresponding to the patterns shown in (a), calculated based on Sherrer equation.

Figure 4.5a shows the voltammograms of the as-prepared and various annealed catalysts. The H_{upd} regions shrank as the annealing temperature increased, indicating the reduction of electrochemical surface area (figure 4.5b). The change in surface area however is not exactly corresponding to the size change observed by TEM and XRD, where it is shown that the particle size was not significantly enlarged after annealing at 500 °C, but the surface area decrease started for

annealing down to 300 °C. The divergence could be clarified, assuming that the annealing at moderate temperatures (≤ 500 °C) would not induce massive particle sintering, but can still reduce surface roughness of the particles compared to non-annealed NPs. The latter effect is not only to be reflected by the change of surface area, but more prominent in activity improvement since it diminishes surface defects, relaxes low-coordinated surface sites, lowers the oxophilicity and enhance the stability of the surface. In addition, at the moderate temperatures (400–500 °C) the compositional profile of NPs in the near surface region could be changed due to Pt segregation, which will be detailed in the next section.

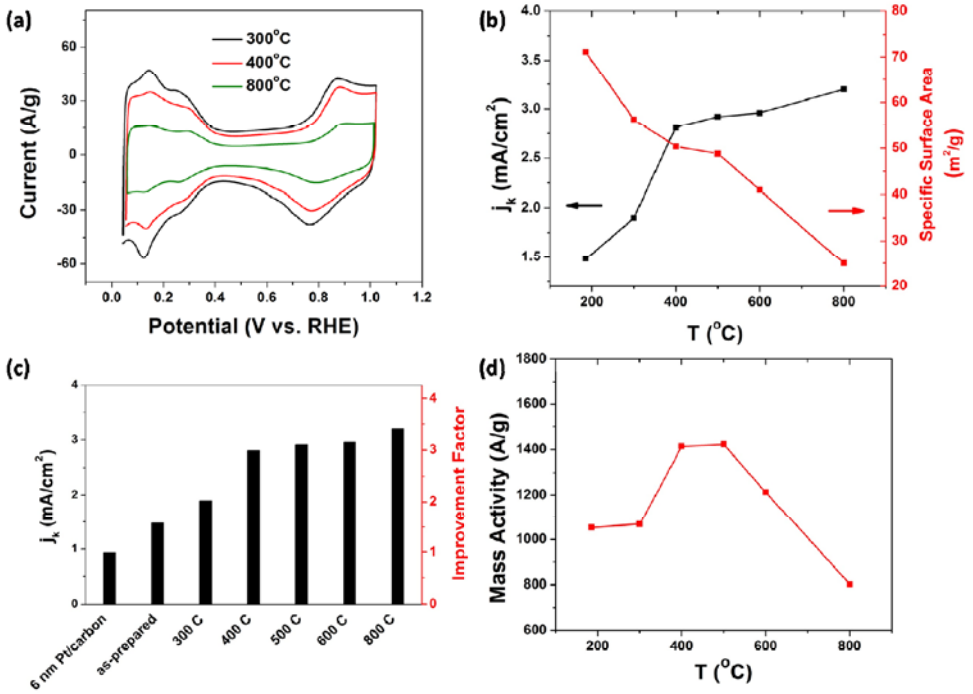

Figure 4.5 (a) Voltammograms recorded for Pt_3Co NP catalysts annealed at different temperatures. (b) The plots of specific activity and specific surface area versus annealing temperature. (c) The summary of specific activities and corresponding improvement factors against the Pt/C catalyst. (d) The plot of mass activity versus the annealing temperature.

Another important finding is related to the position of the oxidation peak (~0.9 V in the anodic scan) and the reduction peak (~0.8V in the cathodic scan). For the Pt_3Co/C annealed at 400 °C and higher temperatures these peaks exhibit a small yet still visible positive shift versus the as-prepared and 300 °C annealed catalyst, with the extent of shift slightly ascending as the annealing temperature increases. This

indicates reduced adsorption of blocking oxygenated species on those annealed catalysts, which has a direct impact on the ORR reaction kinetics as given by the pre-exponential factor of the conventional transition-state-theory rate expression. [45] It is evidenced by the trend in specific activities recorded for differently treated Pt_3Co/C NPs, as shown by the black curve in figure 4.5b. All of the annealed catalysts have ORR activities higher than the as-prepared one. While raising the annealing temperature leads to precipitous activity enhancement for the low-temperature region, the improvement trend significantly slows down for T > 400 ^{o}C.Aspecific activity boost of almost 1 mA cm^{2} was obtained for temperature elevation from 300 to 400 ^{o}C, implying that surface segregation may have happened. Compared to a state-of-the-art Pt/C catalyst with relatively large particle size (5 nm Pt, Tanaka), the as-prepared Pt_3Co/C shows an enhancement factor of about 1.5 times, while a moderate annealing temperature (400–500 ^{o}C) can give a total ORR activity enhancement up to 3 times larger (figure 4.5c) without inducing significant particle sintering.

The descending trend in specific surface area for different annealing temperatures is followed by an ascending trend in specific activities, generating volcano shape in the dependence of mass activity on annealing temperature (figure 4.5c). The optimal treating conditions to obtain the maximal mass activity were thus found to be in the range of 400–500 ^{o}C in this case (figure 4.5d).

It is important to point out that the activities presented here are much higher than those reported in the literature for PtCo alloy catalysts prepared by conventional co-precipitation or impregnation methods, and also higher than the values we measured for commercial PtCo/C. [14, 46] This suggests that the NPs obtained from organic solution synthesis may have a more homogeneous alloy composition than those prepared by the conventional methods.

4.3.4 Modeling and mechanisms

Further insight into the effects of particle size and annealing on the ORR activity was provided by modeling the nanostructure evolution depending on the size and annealing temperatures. Previous work on extended surfaces has demonstrated that element segregation in PtM bimetallic alloys can generate surface structures with Pt-skin layer and transition metal enriched subsurface layer. [12, 13] Since then many attempts have been dedicated to achieve the structure architecture at nanoscale. Chen *et al.* [46] treated the commercial Pt_3Co/C catalyst in a controlled

manner with acid leaching and high-temperature annealing(~1000 K) sequentially, and claimed the observation of ''sandwich-segregation'' structures with Pt-rich surface and Co-rich subsurface layer which was, however, associated with the particle aggregation and size increase after the annealing. An ORR activity enhancement of ~4 times was observed and ascribed to the surface segregation in this report. Mayrhofer *et al.* [47] applied CO annealing to induce surface segregation for Pt_xCo_y/Pt core/shell NPs. Though an activity improvement factor of ~2.5 was reported, the required potential cycling in an alkaline electrolyte complicates the catalyst preparation procedures and limits the potential of scaling up this approach. Nonetheless, a correlation of the pretreatment conditions of Pt-bimetallic catalysts with their catalytic performance is yet ambiguous and challenging, while its significance has been well recognized for development and synthesis of advanced catalysts for fuel-cell reactions.

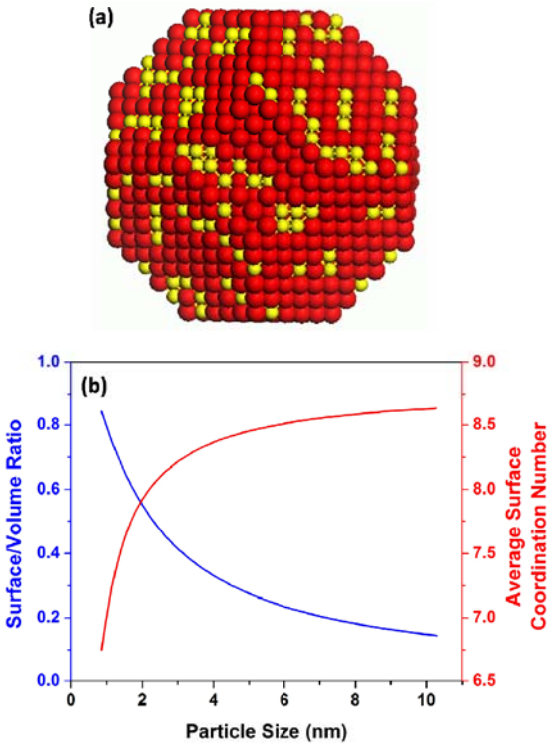

Figure 4.6 (a) Atomic model of a cubo-octahedral Pt_3Co. Red spheres illustrate the position of Pt atoms; yellow spheres depict the Co atoms. NP of fcc phase. (b) The statistical results of the ratio between the number of atoms on the surface and that of the whole particle (left axis), and the average coordination number of surface atoms (right axis) as functions of the particle size.

In order to pave the way toward a fundamental understanding of the electrochemical results depicted above, we first set up an atomic model of the Pt_3Co NPs. figure 4.6a shows a cubo-octahedral Pt_3Co NP with fcc lattice. The lattice constant adopts a value of 3.831 Å. [48] As the number of atoms in the particle enlarges, the particle size increases, and the ratio of surface atoms in the particle (surface/volume ratio, figure 4.6b) decreases, corresponding to reduced specific surface area (figure 4.2c). Another consequence of the size dependence is the average surface coordination number of the particle increases with the particle size. While a 3 nm Pt_3Co NP has an average surface coordination number of ~8.2, a 9 nm particle has a number of over 8.6. Such differences in coordination might have a substantial influence on the surface adsorption properties, as revealed by the voltammograms and ORR activities of Pt_3Co NPs of different sizes (figure 4.2). While the particle size effect can be resolved clearly and quantitatively, it is not that straightforward to identify the correlation between annealing temperature and ORR activity. The possibility of crystal phase divergence, as reported by Schulenburg *et al.* [44] has been excluded by the XRD analyses of the catalysts after annealing (figure 4.4), which also show that 1 the particle size effect is unlikely to contribute the observed activity enhancement for annealing at and below 500 ^{o}C. Therefore, the nanostructure, composition profile and element segregation seem to be dominant in this case. To investigate this we have carried out simulations of element segregation in the NPs with and without low-coordinated surface sites. Starting from a 4.3 nm Pt_3Co NP of perfect cubo-octahedral shape and with randomly distributed Pt and Co atoms, figure 4.7a and b show the structure of a single NP after a sequential 2 million steps of Monte Carlo simulation at 400 ^{o}C. The resultant Pt concentrations are 99 at.% in the outermost surface layer, 44 at.% in the second sub-surface layer, and 92 at.% in the third sub-surface layer. On the contrary, for a particle of the same shape and size but with the outermost surface layer to be amorphous, the simulation resulted in Pt ratios of 70 at.% in the outermost surface layer, 80 at.% in the sub-surface layer, and 71 at.% in the third sub-surface layer (figure 4.7c and d). The presence of Co on the surface for NPs with an amorphous outermost atomic layer thus implies that the surface segregation should happen after the surface relaxation stage.

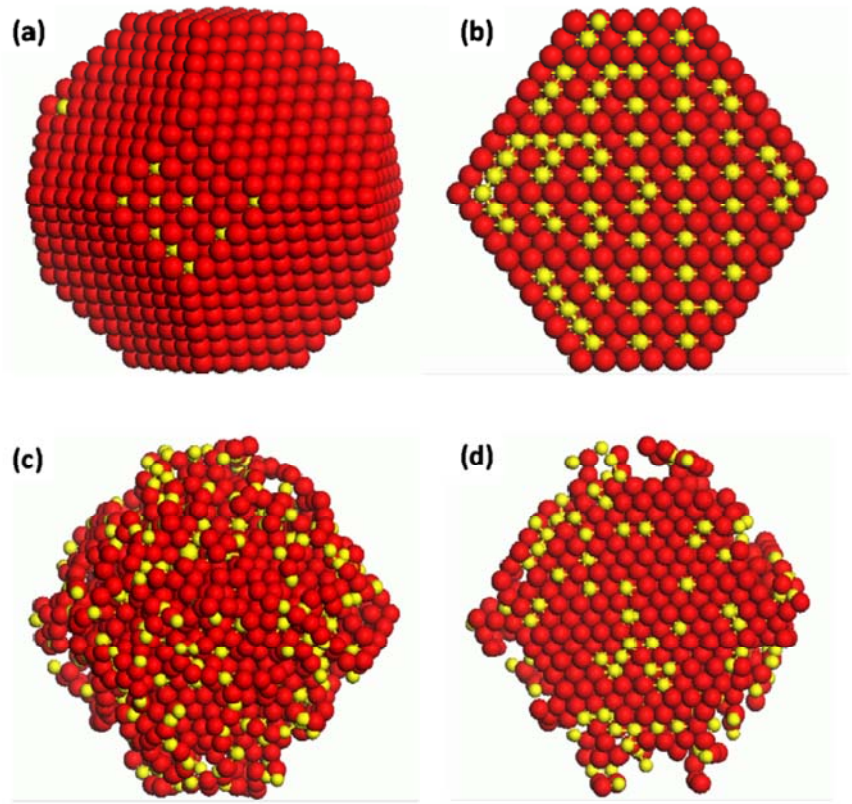

Figure 4.7 Monte Carlo simulation results of surface segregation for the Pt_3Co particle: (a), (b) without surface defect; (c), (d) with the first atomic layer amorphous. Here the right-side images are cross-section views of the particles represented in 3D on the left.

Therefore, we propose that the annealing-temperature-dependent ORR performance can be interpreted in a sequential stage mechanism. Upon annealing, the first response of the bimetallic NPs could be surface relaxation, diminishing low-coordinated surface sites. This process can be initiated at rather low temperatures (*e.g.*,<300 °C) and prevailing the activity enhancement in this temperature range. As the temperature is raised(~400 °C), bulk atomic diffusion is accelerated and element segregation alternates the particle concentration profile to be with surface enriched in Pt and subsurface in Co, providing the activity boost that originates from the modification of surface electronic structure and adsorption properties by the subsurface transition metal atoms, as well as protection of Co dissolution. [13] Further specific activity enhancement at rather high temperatures (>500 °C) can be ascribed to particle size increase caused by catalyst aggregation and sintering.

4.4 Summary

We have prepared Pt_3Co nanoparticle catalysts with size control, and investigated the effects of particle size and annealing temperature on their catalytic properties toward the oxygen reduction reaction. Based on the Monte Carlo simulation of the nanoparticle structure and element segregation, we have been able to correlate the particle size effect with the average surface coordination number, as well as the pretreatment annealing temperature with the particle surface relaxation and segregation. The developed strategies and proposed mechanisms thus shed a light on the fundamental understanding of activity enhancement in Pt-bimetallic alloy catalysts, which could also be generalized to the synthesis of advanced catalysts for other applications.

References

[1] S. D. Bader, Reviews of Modern Physics. 78 (2006) 1.

[2] C. Desvaux, C. Amiens, P. Fejes, P. Renaud, M. Respaud, P. Lecante, E. Snoeck, and B. Chaudret, Nature Materials. 4 (2005) 750.

[3] W. S. Seo, J. H. Lee, X. M. Sun, Y. Suzuki, D. Mann, Z. Liu, M. Terashima, P. C. Yang, M. V. McConnell, D. G. Nishimura, and H. J. Dai, Nature Materials. 5 (2006) 971.

[4] S. H. Sun, C. B. Murray, D. Weller, L. Folks, and A. Moser, Science. 287 (2000) 1989.

[5] C. Wang, Y. L. Hou, J. M. Kim, and S. H. Sun, Angewandte Chemie-International Edition. 46 (2007) 6333.

[6] S. Link, Z. L. Wang, and M. A. El-Sayed, Journal of Physical Chemistry B. 103 (1999) 3529.

[7] Y. G. Sun, B. Wiley, Z. Y. Li, and Y. N. Xia, Journal of the American Chemical Society. 126 (2004) 9399.

[8] C. Wang, S. Peng, R. Chan, and S. H. Sun, Small. 5 (2009) 567.

[9] C. Wang, H. G. Yin, R. Chan, S. Peng, S. Dai, and S. H. Sun, Chemistry of Materials. 21 (2009) 433.

[10] T. Toda, H. Igarashi, H. Uchida, and M. Watanabe, Journal of the Electrochemical Society. 146 (1999) 3750.

[11] J. Greeley and M. Mavrikakis, Nature Materials. 3 (2004) 810.

[12] V. R. Stamenkovic, B. S. Mun, M. Arenz, K. J. J. Mayrhofer, C. A. Lucas, G. F. Wang, P. N. Ross, and N. M. Markovic, Nature Materials. 6 (2007) 241.

[13] V. R. Stamenkovic, B. Fowler, B. S. Mun, G. F. Wang, P. N. Ross, C. A. Lucas, and N. M. Markovic, Science. 315 (2007) 493.

[14] H. A. Gasteiger, S. S. Kocha, B. Sompalli, and F. T. Wagner, Applied Catalysis B-Environmental. 56 (2005) 9.

[15] P. J. Ferreira, G. J. la O', Y. Shao-Horn, D. Morgan, R. Makharia, S. Kocha, and H. A. Gasteiger, Journal of the Electrochemical Society. 152 (2005) A2256.
[16] Y. D. Qian, W. Wen, P. A. Adcock, Z. Jiang, N. Hakim, M. S. Saha, and S. Mukerjee, Journal of Physical Chemistry C. 112 (2008) 1146.
[17] J. N. Soderberg, A. H. C. Sirk, S. A. Campbell, and V. I. Birss, Journal of the Electrochemical Society. 152 (2005) A2017.
[18] S. Tominaka, T. Momma, and T. Osaka, Electrochimica Acta. 53 (2008) 4679.
[19] Y. Saejeng and N. Tantavichet, Journal of Applied Electrochemistry. 39 (2009) 123.
[20] S. Mukerjee and S. Srinivasan, Journal of Electroanalytical Chemistry. 357 (1993) 201.
[21] S. Mukerjee, S. Srinivasan, M. P. Soriaga, and J. Mcbreen, Journal of Physical Chemistry. 99 (1995) 4577.
[22] U. A. Paulus, A. Wokaun, G. G. Scherer, T. J. Schmidt, V. Stamenkovic, N. M. Markovic, and P. N. Ross, Electrochimica Acta. 47 (2002) 3787.
[23] U. A. Paulus, A. Wokaun, G. G. Scherer, T. J. Schmidt, V. Stamenkovic, V. Radmilovic, N. M. Markovic, and P. N. Ross, Journal of Physical Chemistry B. 106 (2002) 4181.
[24] K. Kinoshita, Journal of the Electrochemical Society. 137 (1990) 845.
[25] K. J. J. Mayrhofer, B. B. Blizanac, M. Arenz, V. R. Stamenkovic, P. N. Ross, and N. M. Markovic, Journal of Physical Chemistry B. 109 (2005) 14433.
[26] Chapter 3 of this Thesis
[27] Y. W. Jun, J. S. Choi, and J. Cheon, Angewandte Chemie-International Edition. 45 (2006) 3414.
[28] C. B. Murray, C. R. Kagan, and M. G. Bawendi, Annual Review of Materials Science. 30 (2000) 545.
[29] B. L. Cushing, V. L. Kolesnichenko, and C. J. O'Connor, Chemical Reviews. 104 (2004) 3893.
[30] C. Burda, X. B. Chen, R. Narayanan, and M. A. El-Sayed, Chemical Reviews. 105 (2005) 1025.
[31] R. Ferrando, J. Jellinek, and R. L. Johnston, Chemical Reviews. 108 (2008) 845.
[32] E. V. Shevchenko, D. V. Talapin, A. L. Rogach, A. Kornowski, M. Haase, and H. Weller, Journal of the American Chemical Society. 124 (2002) 11480.
[33] Z. F. Liu, M. Shamsuzzoha, E. T. Ada, W. M. Reichert, and D. E. Nikles, Journal of Power Sources. 164 (2007) 472.
[34] Chapter 2 of this Thesis.
[35] M. I. Baskes, Physical Review B. 46 (1992) 2727.
[36] M. I. Baskes and R. A. Johnson, Modelling and Simulation in Materials Science and Engineering. 2 (1994) 147.
[37] G. F. Wang, M. A. Van Hove, P. N. Ross, and M. I. Baskes, Journal of Chemical Physics. 122 (2005).
[38] G. F. Wang, M. A. Van Hove, P. N. Ross, and M. I. Baskes, Journal of Chemical Physics. 121 (2004) 5410.
[39] G. F. Wang, M. A. Van Hove, P. N. Ross, and M. I. Baskes, Journal of Physical Chemistry B. 109 (2005) 11683.
[40] J. T. Ren and R. D. Tilley, Journal of the American Chemical Society. 129 (2007) 3287.
[41] C. Wang, H. Daimon, T. Onodera, T. Koda, and S. H. Sun, Angewandte Chemie-International Edition. 47 (2008) 3588.

[42] H. Yano, J. Inukai, H. Uchida, M. Watanabe, P. K. Babu, T. Kobayashi, J. H. Chung, E. Oldfield, and A. Wieckowski, Physical Chemistry Chemical Physics. 8 (2006) 4932.
[43] H. Liu, W. Li, and A. Manthiram, Applied Catalysis B-Environmental. 90 (2009) 184.
[44] H. Schulenburg, E. Muller, G. Khelashvili, T. Roser, H. Bonnemann, A. Wokaun, and G. G. Scherer, Journal of Physical Chemistry C. 113 (2009) 4069.
[45] N. M. Markovic, H. A. Gasteiger, B. N. Grgur, and P. N. Ross, Journal of Electroanalytical Chemistry. 467 (1999) 157.
[46] S. Chen, P. J. Ferreira, W. C. Sheng, N. Yabuuchi, L. F. Allard, and Y. Shao-Horn, Journal of the American Chemical Society. 130 (2008) 13818.
[47] K. J. J. Mayrhofer, V. Juhart, K. Hartl, M. Hanzlik, and M. Arenz, Angewandte Chemie-International Edition. 48 (2009) 3529.
[48] P. Villars and L. D. Calvert, Pearson's Handbook of Crystallographic Data for Intermetallic Phases, ASM International, Materials Park, OH, 1991.